Science Arts & Métiers (SAM)

is an open access repository that collects the work of Arts et Métiers Institute of Technology researchers and makes it freely available over the web where possible.

This is an author-deposited version published in: https://sam.ensam.eu
Handle ID: .http://hdl.handle.net/10985/19398

To cite this version :

Mariem YAICH, Yessine AYED, Zoubeir BOUAZIZ, Guénaël GERMAIN - A 3D Numerical Analysis of the Chip Segmentation Mechanism and the Side Burr Formation During the Ti6Al4V Alloy Machining - 2020

Any correspondence concerning this service should be sent to the repository Administrator : scienceouverte@ensam.eu

Arts et Métiers Institute of Technology

A 3D numerical analysis of the chip segmentation mechanism and the side burr formation during the Ti6Al4V alloy machining

M.Yaich[1], Y.Ayed[2], Z.Bouaziz [3], G.Germain [4]

[1] Ecole Nationale d'Ingénieurs de Sfax, LMFAM, 3035 Sfax, Tunisia
Arts et Métiers ParisTech, LAMPA, 2 bd du Ronceray, 49035 Angers CEDEX, France

Mariem.yaich@enis.tn

[2] ParisTech, LAMPA, 2 bd du Ronceray, 49035 Angers CEDEX, France

Yessine.ayed@ensam.eu

[3] Ecole Nationale d'Ingénieurs de Sfax, MFAM, 3035 Sfax, Tunisia

Zoubeir.bouaziz@gmail.com

[4] ParisTech, LAMPA, 2 bd du Ronceray, 49035 Angers CEDEX, France

Guenael.germain@ensam.eu

Abstract. A 3D finite element modeling of the orthogonal turning process was curried out in the current study. It aims to carefully investigate the mechanisms controlling the chip segmentation and the crack propagation direction in the case of the Ti6Al4V machining. Coupled temperature-displacement numerical simulations were performed in the software Abaqus®/Explicit, under different cutting conditions. The instantaneous distribution of numerical temperatures and damage, along the width of cut, was investigated. High plastic strains, temperatures and pronounced damage were predicted in the median plane of the workpiece, mainly in the shear bands at the tool tip vicinity. Whereas, a reduction of their values was noted while moving toward the chip sides and its upper surface. The 3D numerical simulations pointed out that the orthogonal machining resulted in an increase of the chip width, in addition to the material flow along the X and Y directions. The quantitative analysis of the side burr formation highlighted its sensitivity to the cutting conditions. The definition of high feed rates resulted in pronounced material flow in the workpiece edges, thus the modeling of wider chip. The present study concluded that the chip segmentation is a 3D mechanism. In addition, it pointed out the limitations of the 2D numerical simulations, as well as the inadequacy of the plain strain hypothesis, even in the case of the modeling the orthogonal machining.

Keywords: machining; Abaqus; Ti6Al4V titanium alloy; numerical analysis; chip; side burr

1 Introduction

The machining process of materials with poor machinability, like the titanium alloys (Veiga et al. 2013), is still problematic for both industrials and researchers. Significant material deformation is encountered under high strain rates and induces the temperature rise in the cutting zones. Due to the low conductivity and the pronounced chemical affinity of machined material with the cutting tools, a concentrated and important heating was generated in the cutting zones. It influenced on the tool life and it accelerated its wear (Arrazola et al. 2009). Despite the use of equipment with high precision, the experimental investigation of several instantaneous and local physical phenomena, taking place in very thin cutting zones, is still very expensive and not precise enough (Daoud et al. 2015). Furthermore, the significant thermomechanical coupling heavily limited the efficiency of experimental tests. Therefore, the definition of numerical approaches, in addition to the experimental analysis, has been required to provide valuable information, thus to deal with the severe loading conditions following the machining of difficult to-cut materials (Ali et al. 2014). These approaches has enabled the investigation of transient phenomena and pronounced nonlinearity involved during the chip formation. Furthermore, the valuable advances in the numerical simulations, giving rise to several modeling techniques (finite element (FE) method, discrete element method, smoothed particle hydrodynamics, material point method), have encouraged their use. Literature review highlighted the wide spread adoption of the finite element method, based on the special discretization of the model geometry. The availability of powerful FE commercial codes (Abaqus®, Deform®, AdvantEdge®, Forge®, etc.) explains its common use in the last decades.

Several investigations of the literature (Nouari and Makich 2014; Yaich 2017; Zang et al. 2017) have highlighted the formation of serrated chip, when machining the Ti6Al4V alloy, even when low cutting conditions have been defined. In fact, an enhanced understanding of the several phenomena following the chip segmentation has been required to increase the material machinability. The experimental observations of Pottier et al (Pottier et al. 2014) have been focused on the chip formation process. This latter has been divided into three main sub-processes: compression, localization/propagation and sliding. Despite the adoption of advanced experimental devices (high frame rate camera and optical microscopy) and carrying out in-situ and post-mortem observations, the accurate determination of the direction of the deformation/crack propagation within the chip has been not allowed. The authors have required the definition of numerical analysis for valuable information.

Indeed, the current paper focuses on investigating the phenomena controlling the chip serration. A set of 3D finite element simulations was set up in the software Abaqus®/Explicit to model the orthogonal machining of the Ti6Al4V alloy under several cutting conditions. The distribution of temperatures, plastic strains and damage was investigated. The numerical results corresponding to two different

planes of the workpiece, the medium and the side edge planes, were used to determine the sub-processes of the chip segmentation. The sensitivity of the chip width to the cutting conditions was also studied.

2 Numerical model

A 3D numerical model was set up to simulate the Ti6Al4V orthogonal machining. The Lagrangian formulation integrated in the FE software Abaqus®/Explicit was defined. A fully coupled temperature-displacement analysis was performed. The model geometry was discretized with the 8-node 3D thermally coupled continuum elements (C3D8RT) with reducer integration. The geometry of the tungsten carbide cutting tool and its physical properties were grouped in Table 1 and Table 2, respectively. To reduce the mesh distortion mainly encountered in the cutting zones because of the severe contact conditions induced in the chip-tool-workpiece interfaces, the workpiece was divided in three tied parts (see Fig. 1): the uncut chip part (P_1), the tool passage part (P_2) and the workpiece support (P_3).

Table 1. Cutting conditions and tool geometry

Cutting conditions	
Cutting speed V_c (m/min)	45_75
Uncut chip thickness f (µm)	0.15_0.3
Width of cut a_p (mm)	3
Tool geometry	
Rake angle γ (°)	6
Clearance angle α (°)	7
Edge inclination angle λ_s (°)	0
Edge entering angle κ_r (°)	90
Cutting edge radius r_b (µm)	20

To predict the nonlinear ductile behavior of the Ti6Al4V alloy, the Johnson-Cook (JC) constitutive models (Johnson and Cook 1983, 1985) were defined to the workpiece. These criteria were commonly used the fact that they take into account the effects of the strain hardening, the viscosity, the temperature distribution and the damage initiation on the machined material (see Eq.(1-3)). The damage evolution laws (Eq.(4-5)) were used to predict the progressive degradation of elements mesh, which is induced in the strain localization zones, , while minimizing the dependency of the FE solution on the mesh. We note that a rigid cutting tool was considered for all numerical simulations. The Coulomb-Tresca friction criterion (see Eq.(6)) was used to model the mechanical contact conditions taking place between the cutting tool and the workpiece. Only the effects of the friction

and the plastic deformation of the workpiece material on the heat generation, thus on the temperature rise, were considered in the current study.

Table 2. Physical properties of the cutting tool and the workpiece (Ducobu et al. 2016)

Physical parameters	Tool	Workpiece
Density ρ (kg/m^3)	15 000	4 430
Specific heat C_p (J/kg/K)	203	580
Thermal conductivity λ (W/m/K)	46	7.3
Thermal expansion α_p (µm.m/K)	4.7×10^{-6}	8.6×10^{-6}
Elastic modulus, E (GPa)	–	113.8
Poisson's ratio, v	–	0.342
Inelastic heat friction, η_p	–	0.9
Room temperature, T_{room} (K)	293	293
Melt temperature, T_{melt} (K)	–	1943

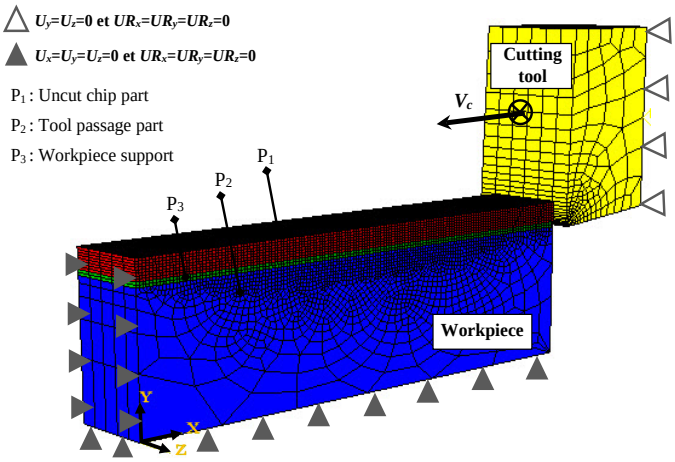

Fig. 1 Model geometry and boundary conditions

$$\sigma = \left(A + B\left(\varepsilon_p\right)^n\right) \times \left(1 + C\ln\left(\frac{\dot{\varepsilon}_p}{\dot{\varepsilon}_0}\right)\right) \times \left(1 - \left(\frac{T - T_{room}}{T_{melt} - T_{room}}\right)^m\right) \quad (1)$$

where, A, B, n, C and m are the JC plasticity coefficients. Their corresponding values are grouped in Table 3. T_{room} and T_{melt} are the reference and the room temperatures respectively. $\dot{\varepsilon}_0$ is the reference strain rate.

$$w_{JC} = \sum \frac{\Delta\varepsilon_p}{\varepsilon_{i0}} \quad (2)$$

where, $\Delta\varepsilon_p$ is the accumulated plastic strain. ε_{i0} is the plastic strain at the damage initiation and it computed as follow:

$$\varepsilon_{i0} = \left(D_1 + D_2 \exp\left(D_3 \frac{\sigma_h}{\sigma_{vm}} \right) \right) \times \left(1 + D_4 \ln\left(\frac{\dot{\varepsilon}}{\dot{\varepsilon}_0} \right) \right) \times \left(1 + D_5 \left(\frac{T - T_{room}}{T_{melt} - T_{room}} \right) \right) \quad (3)$$

where, $D_{1\sim5}$ are the JC damage coefficients and they are given by Table 3. σ_h and σ_{VM} are the hydrostatic and the Von Mises stresses, respectively.

Table 3. JC constitutive coefficients (Nemat-Nasser et al. 2001; Zhang et al. 2011)

JC plasticity coefficients				
A (MPa)	*B* (MPa)	*n*	*C*	*m*
1119	838,6	0,473	0,019	0,643
JC damage coefficients				
D_1	D_2	D_3	D_4	D_5
-0.09	*0.25*	*-0.5*	*0.014*	*3.87*

$$\left(D_{ev}\right)_{Linear} = \frac{\bar{u}_p}{\bar{u}_f} = \bar{u}_p \times \frac{\tilde{\sigma}}{2G_f} \quad (4)$$

$$\left(D_{ev}\right)_{exponential} = 1 - exp\left(-\int_0^{\bar{u}_p} \left(\frac{\tilde{\sigma}}{G_f} \right) \times d\bar{u}_p \right) \quad (5)$$

where, $\left(D_{ev}\right)_{Linear}$ and $\left(D_{ev}\right)_{exponential}$ are the damage variables for linear and exponential failure evolutions, respectively. $\bar{u}_f$ is the plastic displacement at failure, G_f is the fracture energy and $\tilde{\sigma}$ is the flow stress at the damage initiation.

$$\tau_f = \begin{cases} \mu \times \sigma_n & (if\ \mu \times \sigma_n < \tau_{\max}) \\ \tau_f = \tau_{\max} = m_{Tresca} \times k & (if\ \mu \times \sigma_n \geq \tau_{\max}) \end{cases} \quad (6)$$

where, τ_f, μ, σ_n, m_{Tresca} and k are the shear stress, the Coulomb's coefficient, the normal friction stress, the Tresca factor and the yield stress, respectively.

3 Results and discussion

Fig. 2 illustrates the chip morphology predicted for a cutting speed and a feed rate of 45 m/min and 0.3 mm/rev. A material flow along all directions was obtained when the cutting tool penetrated in the workpiece. For both modeled sections $\left(Z = 0\ mm\ \ or\ \ Z = \pm 0.25\ mm\right)$, high equivalent plastic strains were predicted in the

shear bands, mainly close to the inner chip surface that was in contact with the tool rake face. In addition, a slight mismatch between the chip morphology predicted in the two sections was highlighted. Less serrated chip was modeled in the workpiece sides $\left(Z = \pm 0.25mm\right)$, where the removed material was also deformed along the width of cut direction and it the side burrs formation.

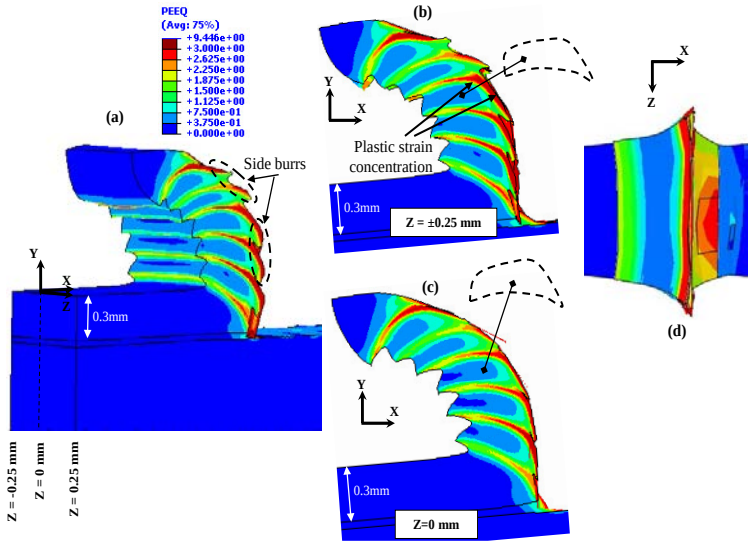

Fig. 2 Chip morphology and equivalent plastic strain distribution in different sections: (a) 3D chip, (b) chip sides, (c) median plane and (d) XZ plane (V_c = 45 m/min and f = 0.3 mm/rev)

To explain these preliminary ascertainments, a detailed analysis of mechanisms controlling the chip segments formation was performed. The instantaneous evolution of temperatures was investigated. Fig. 3 shows a temperature rise in the chip, mainly in its inner surface in contact with the tool edge radius, where a heat concentration in the median plane $\left(Z = 0\ mm\right)$ was underlined. The temperatures furthest from this zone were the lowest. With the progressive cutting tool penetration in the workpiece, the computed temperatures evolved along the shear band to reach the upper surface of the chip and its sides. The non-uniform temperature distribution along the shear plane and the Z-direction was mainly due to the contact friction conditions.

For important cutting time, the computed temperature was accentuated and it reached 1000 K (see Fig. 4 (c-d)). Moreover, a significant heat propagation toward the upper chip surface was noted. A thermally extended affected zone (TAZ) was predicted, which thickness increased with the definition of the highest feed rates.

In addition, the material flow along the workpiece sides was heavily influenced by the feed rate. Fig. 5 illustrates a significant increase of the average width of the

side burr for f = 0.3 mm/rev, under both investigated cutting speeds. It was about 40% the modeled feed rate.

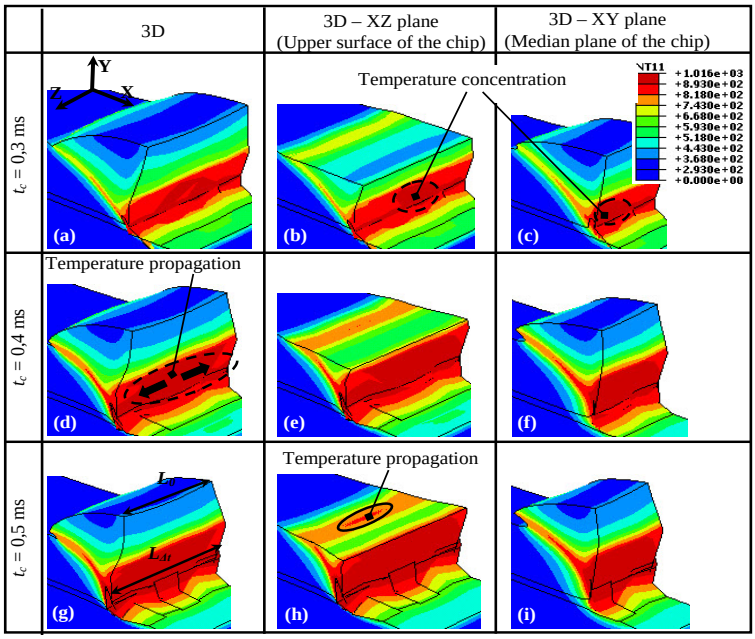

Fig. 3 Instantaneous temperature distribution in the chip for different observation planes (V_c = 45 m/min and f = 0.3 mm/rev)

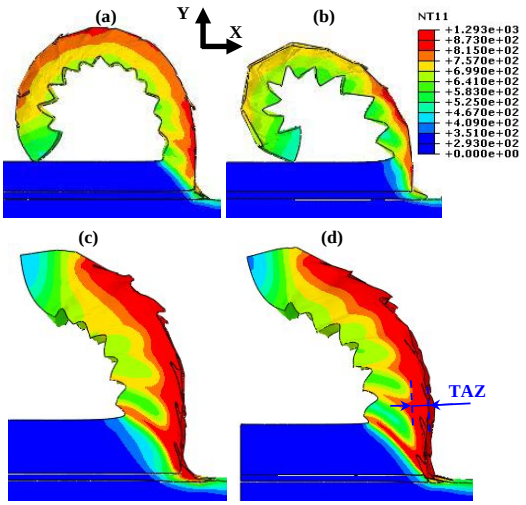

Fig. 4 Effect of the cutting conditions on the temperature distribution: (a) V_c = 45 m/min and f = 0.15 mm/rev, (b) V_c = 75 m/min and f = 0.15 mm/rev, (c) V_c = 45 m/min and f = 0.3 mm/rev and (d) V_c = 75 m/min and f = 0.3 mm/rev

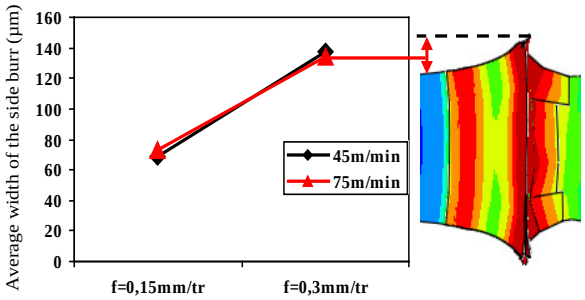

Fig. 5 Effect of the cutting conditions on the side burr

The instantaneous and local distribution of the damage variable (*SDEG*) in the chip was studied to better understand the chip segmentation process. Numerical chip illustrated by Fig. 6 underlined that, for both investigated planes, the segments formation was controlled by three main sub-processes:

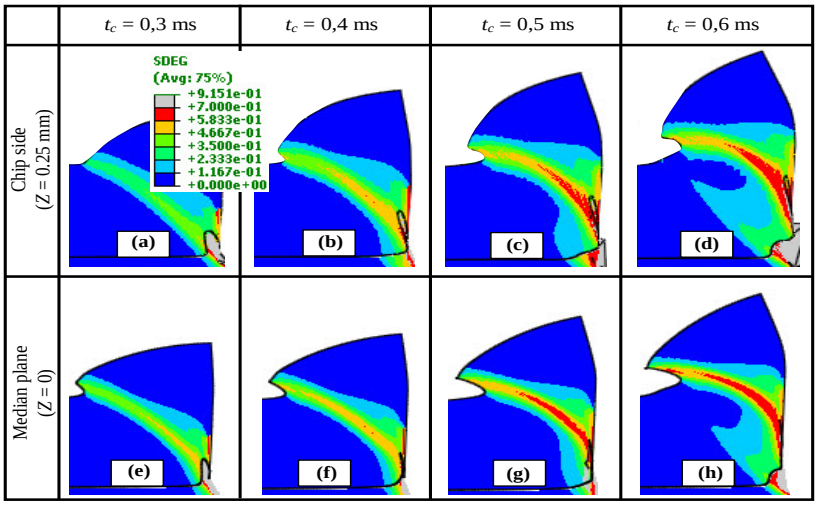

Fig. 6 Instantaneous damage distribution in the chip as a function of the observation plane (V_c = 45 m/min and f = 0.3 mm/rev)

- Compression: The machined material was initially compressed without being damaged. An increase of the damage variable was noted in the tool tip vicinity, while almost undamaged material was modeled away from this contact interface.
- Localization and propagation: More accentuated and propagated sticking contact was involved in the tool-chip interface, following the progressive penetration of the cutting tool in the workpiece. This explains the important and local heating of the bottom chip surface, which was in contact with the rake tool face, illustrated by Fig. 3. These pronounced thermomechanical conditions

resulted in the damage rise. The most important and concentrated *SDEG* were reached in the median plane, notably in the primary shear band just around the tool tip. Therefore, more pronounced sliding of the chip along the shear plane was obtained, giving rise to slight distinction in the segment geometry from one modeled plane to another.

- Ejection: The chip slid upwards on the tool rake face, until the total formation of the first chip segment. Thereby, a second segment began to form.

The comparison of numerical results illustrated in Fig. 6 (a) and (e) highlighted that, for the same cutting time (t_c = 0.3 ms), the chip formation was initiated in the median plane, which was not the case at the chip sides. Similar delay was noted for the other cutting times. This result confirmed the hypothesis of damage propagation from the median plane to the chip sides, which was made by Pottier et al (Pottier et al. 2014).

4 Conclusion

The 3D modeling of the Ti6Al4V orthogonal machining allowed to better understand the multi-physical mechanisms controlling the chip formation. A noticeable mismatch between the distribution and the levels of numerical plastic strains, temperatures and damage variables, which were computed in the workpiece median plane and its sides, was pointed out. A pronounced thermal softening was modeled in the median plane; and it resulted in more concentrated and important damage in narrow shear bands, just around the tool edge. These numerical results demonstrated the crack propagation from the median plane to the workpiece sides, hence the efficiency of the 3D FE modeling. They underlined the inability of the 2D FE modeling to predict the chip formation mechanisms, even in the case of orthogonal machining.

In this study, an increase of the chip width, due to the material flow along the width of cut direction was highlighted. . The modeling of several cutting conditions underlined the sensitivity of side burrs to the feed rate. They became more pronounced, giving rise to additional thermomechanical loads applied to the cutting tool. Although the low intensity of this kind of material flow compared to that obtained in thickness, the consideration of its effect on the machining was required.

References

Ali MH, Ansari MNMNM, Khidhir BA, Mohamed B, Oshkour AA (2014) Simulation machining of titanium alloy (Ti-6Al-4V) based on the finite element modeling. J Brazilian Soc Mech Sci Eng 36:315–324. doi: 10.1007/s40430-013-0084-0

Arrazola PJ, Garay A, Iriarte LM, Armendia M, Marya S, Le Maître F (2009) Machinability of titanium alloys (Ti6Al4V and Ti555.3). J Mater Process Technol 209:2223–2230. doi: 10.1016/j.jmatprotec.2008.06.020

Daoud M, Jomaa W, Chatelain JE, Bouzid A, (2015) A machining-based methodology to identify materialconstitutive law for finite element simulation. Int J Adv Manuf Technol 77:2019–2033

Ducobu F, Rivière-Lorphèvre E, Filippi E (2016) Material constitutive model and chip separation criterion influence on the modeling of Ti6Al4V machining with experimental validation in strictly orthogonal cutting condition. Int J Mech Sci 107:136–149. doi: 10.1016/j.ijmecsci.2016.01.008

Johnson GR, Cook WH (1985) Fracture characteristics of three metals subjected to various strains, strain rates, temperatures and pressures. Eng Fract Mech 21:31–48

Johnson GR, Cook WH (1983) A constitutive model and data for metals subjected to large strains, high strain rates and high temperatures. Proc. 7th Int. Symp. Ballist. 547:541–547

Nemat-Nasser S, Guo WG, Nesterenko VF, Indrakanti SS, Gu YB (2001) Dynamic response of conventional and hot isostatically pressed Ti-6Al-4V alloys: Experiments and modeling. Mech Mater 33:425–439. doi: 10.1016/S0167-6636(01)00063-1

Nouari M, Makich H (2014) On the Physics of Machining Titanium Alloys: Interactions between Cutting Parameters, Microstructure and Tool Wear. Metals (Basel) 4:335–358. doi: 10.3390/met4030335

Pottier T, Germain G, Calamaz M, Morel A, Coupard D (2014) Sub-Millimeter Measurement of Finite Strains at Cutting Tool Tip Vicinity. Exp Mech 54:1031–1042. doi: 10.1007/s11340-014-9868-0

Veiga C, Davim JP, Loureiro AJR (2013) Review on machinability of titanium alloys: The process perspective. Rev. Adv. Mater. Sci.

Yaich M (2017) Contribution à la fiabilisation de la modélisation numérique de l'usinage de pièces en titane

Zang J, Zhao J, Li A, Pang J (2017) Serrated chip formation mechanism analysis for machining of titanium alloy Ti-6Al-4V based on thermal property. Int J Adv Manuf Technol. doi: 10.1007/s00170-017-0451-6

Zhang YC, Mabrouki T, Nelias D, Gong YD (2011) Chip formation in orthogonal cutting considering interface limiting shear stress and damage evolution based on fracture energy approach. Finite Elem Anal Des 47:850–863. doi: 10.1016/j.finel.2011.02.016